nature COMMUNICATIONS

ARTICLE

Received 28 Dec 2015 | Accepted 28 Apr 2016 | Published 3 Jun 2016

DOI: 10.1038/ncomms11796 OPEN

Interface strain in vertically stacked two-dimensional heterostructured carbon-MoS_2 nanosheets controls electrochemical reactivity

Landon Oakes[1,2], Rachel Carter[1], Trevor Hanken[1], Adam P. Cohn[1], Keith Share[1,2], Benjamin Schmidt[3] & Cary L. Pint[1,2,3]

Two-dimensional (2D) materials offer numerous advantages for electrochemical energy storage and conversion due to fast charge transfer kinetics, highly accessible surface area, and tunable electronic and optical properties. Stacking of 2D materials generates heterogeneous interfaces that can modify native chemical and physical material properties. Here, we demonstrate that local strain at a carbon-MoS_2 interface in a vertically stacked 2D material directs the pathway for chemical storage in MoS_2 on lithium metal insertion. With average measured MoS_2 strain of $\sim$0.1% due to lattice mismatch between the carbon and MoS_2 layers, lithium insertion is facilitated by an energy-efficient cation-exchange transformation. This is compared with low-voltage lithium intercalation for unstrained MoS_2. This observation implies that mechanical properties of interfaces in heterogeneous 2D materials can be leveraged to direct energetics of chemical processes relevant to a wide range of applications such as electrochemical energy storage and conversion, catalysis and sensing.

[1] Department of Mechanical Engineering, Vanderbilt University, Nashville, Tennessee 37235, USA. [2] Interdisciplinary Materials Science Program, Vanderbilt University, Nashville, Tennessee 37235, USA. [3] Vanderbilt Institute of Nanoscale Science and Engineering, Vanderbilt University, Nashville, Tennessee 37235, USA. Correspondence and requests for materials should be addressed to C.L.P. (email: cary.l.pint@vanderbilt.edu).

2D graphene and transition metal dichalcogenide (TMDC) materials have captivated researchers in the past decade owing to a set of unique physical and chemical properties that deviate from their bulk analogues and the exploitation of these properties in broad applications[1]. Specifically for electronics, vertical integration of 2D materials enables logic component design with high on-off ratio and promise for three-dimensional (3D) electronics that progress beyond silicon[2–8]. In semiconductor electronics, engineering 2D TMDC materials using strain applied at an interface has been shown to strongly modulate the bandgap and band structure, which results in modified electrical and optical properties for strained materials[9–14]. For monolayer MoS_2, the bandgap is observed to shift by up to 15 meV under tensile strain of up to 4.8% (ref. 15), and for multilayered WSe_2 the bandgap transitions from indirect to direct under strain of up to 2% (ref. 16). Theoretical efforts have further emphasized strain-enabled broadband absorption and photodetection in MoS_2, even though this has not yet been experimentally realized[17]. The intersection of strain-engineered properties of 2D materials and heterostructured vertically integrated interfaces of 2D materials presents an engaging research area for next-generation electronics. Nonetheless, such materials and research directions remain elusive for many other applications of 2D materials.

On this front, 2D materials and specifically 2D TMDCs have demonstrated excellent performance in a range of electrochemical applications including lithium- and sodium-ion batteries[18–20], photocatalytic conversion[21–23] and biosensing applications[24–26]. Unlike electronic devices, these applications require bulk-like quantities of 2D materials—a challenge aided by recent developments in the liquid exfoliation and assembly of layered TMDCs[27–29]. However, addressing how properties in heterostructured or complex 2D materials can impact chemical processes responsible for electrochemical applications is hampered by uniform material fabrication routes that can be used on scales required for electrochemical measurements. As a result, the impact of strained interfaces in 2D materials on chemical and electrochemical processes remains virtually unstudied. Only recently has an observation emerged that compressive strain on Pt catalysts can improve the oxygen reduction reaction capability of Pt relevant to fuel cells[30]. In this manner, 2D materials provide an ideal test bed for the understanding of how interfaces and strain can impact electrochemical processes, motivated by pioneering efforts in the field of semiconductor electronics.

This is the focus of this report, which documents that interface strain measured over statistical quantities of stacked 2D carbon-MoS_2 heterostructured nanosheets can be directly correlated with distinct differences in chemical processes occurring in 2D materials. In particular, combining optical and electrochemical techniques we demonstrate that strain engineering of interfaces can enable control of the energetic pathway for the chemical conversion of MoS_2 into electrochemically active Mo and Li_2S_n species during reaction with lithium. This highlights the important role that mechanical strain can have in engineering energy storage processes in materials.

Results

Fabrication of interface-strained materials. MoS_2 nanosheets were produced through liquid exfoliation of bulk MoS_2 powders in *n*-methyl-2-pyrrolidone (NMP) solvents and subsequent centrifugation. Transmission electron microscopy (TEM) of a representative exfoliated MoS_2 nanosheet is shown in Fig. 1a,b. Interlayer spacing of $\sim$0.61 nm is observed for MoS_2 nanosheets, with thicknesses ranging from 2–15 atomic layers (Supplementary Fig. 1, Supplementary Note 1). Ultrathin carbon layers are grown directly on the MoS_2 surface through MoS_2 catalysed decomposition of C_2H_2 precursors using a temperature ramp chemical vapour deposition process (Supplementary Fig. 2) that is capable of gram-scale batch processing. This generates vertically stacked architectures where ultrathin carbon layers are formed on both sides of the MoS_2 nanosheets, with a representative TEM image of this architecture shown in Fig. 1c, and corresponding elemental analysis map in Fig. 1d. To produce an appreciable mass of material for electrochemical tests, electrophoretic deposition was used to assemble the vertically stacked carbon-interfaced MoS_2 (C-MoS_2) nanosheets into conformal films on metal substrates from NMP dispersions following chemical vapour deposition (Fig. 1e; Supplementary Fig. 3, Supplementary Note 2). All aspects of synthesis and processing of C-MoS_2 materials are chosen to be compatible with scalable processing, and ongoing research efforts to improve the simplicity and scalability of liquid exfoliation can further improve this[31]. Raman spectroscopy analysis (Fig. 1f) of vertically stacked C-MoS_2 nanosheets indicates that vertical stacks maintain an identical signature of crystalline MoS_2 following the carbon synthesis based on E_{2g} and A_{1g} modes (300–500 cm^{-1}). The carbon layers exhibit a significant amount of sp^3 hybridized carbon atoms ($\sim$1,320 cm^{-1}, or D-band) relative to sp^2 carbon species ($\sim$1,580 cm^{-1}, or G-band). Whereas this indicates the presence of carbon, X-ray photoelectron spectroscopy (XPS) indicates the emergence of both a peak in the sulfur $2p_{3/2}$ and $2p_{5/2}$ spectra at low-binding energies, as well as shoulders in both Mo $3d_{5/2}$ and $3d_{3/2}$ peaks that represent a modulation to the local bonding environment in the crystal (Fig. 1g). Notably, the existence of the low-energy shoulder in the sulfur *2p* and Mo *3d* peaks is consistent with the formation of the metallic 1T-phase of MoS_2 produced from the strain-induced distortion of sulfur atoms observed previously (Supplementary Fig. 4, Supplementary Note 3)[32]. This analysis collectively supports the formation of a distinct carbon-MoS_2 stacked interface, where mismatch of the in-plane lattice spacing between MoS_2 and carbon will induce significant interface strain that propagates into the MoS_2 nanosheet from the C-MoS_2 interface.

To assess strain in the vertically stacked 2D material, statistical Raman spectroscopy mapping comprising over 200 individual scans in separate areas was performed on the E_{2g} and A_{1g} modes of MoS_2, which are highly sensitive to tensile or compressive strain[33–35]. (Fig. 2a,b) On the basis of the peak-to-peak analysis of Raman mode distributions, blue-shifts of $\sim$0.66 cm^{-1} and $\sim$0.59 cm^{-1} were observed for the E_{2g} and A_{1g} modes, respectively. Asymmetry in these modes is expected and attributed to stronger electronic coupling to the A_{1g} mode[36]. This yields an $\sim$0.1–0.2% compressive strain based on relative A_{1g} mode shifts in accordance with previous studies[9,34], supporting the presence of interface-induced compressive strain on the MoS_2 material. This is further confirmed using X-ray diffraction which demonstrates a similar $\sim$0.1% compressive strain due to vertical stacking based on analysis of the (100) and (110) low-index planes of MoS_2 (Fig. 2c). We anticipate this measured strain to be present at both the interface and on the interior of the nanosheets as they possess a thickness well below the critical layer thickness at which strain relaxation occurs[37].

Controlling electrochemical processes using strain. To assess how the vertically stacked architecture and interface strain influences electrochemical processes, we combined electrophoretically assembled vertically stacked 2D C-MoS_2 nanosheets with Li metal electrodes, and a 1.0 M lithium hexafluorophosphate solution in ethylene carbonate and diethyl carbonate electrolyte, and compared the electrochemical

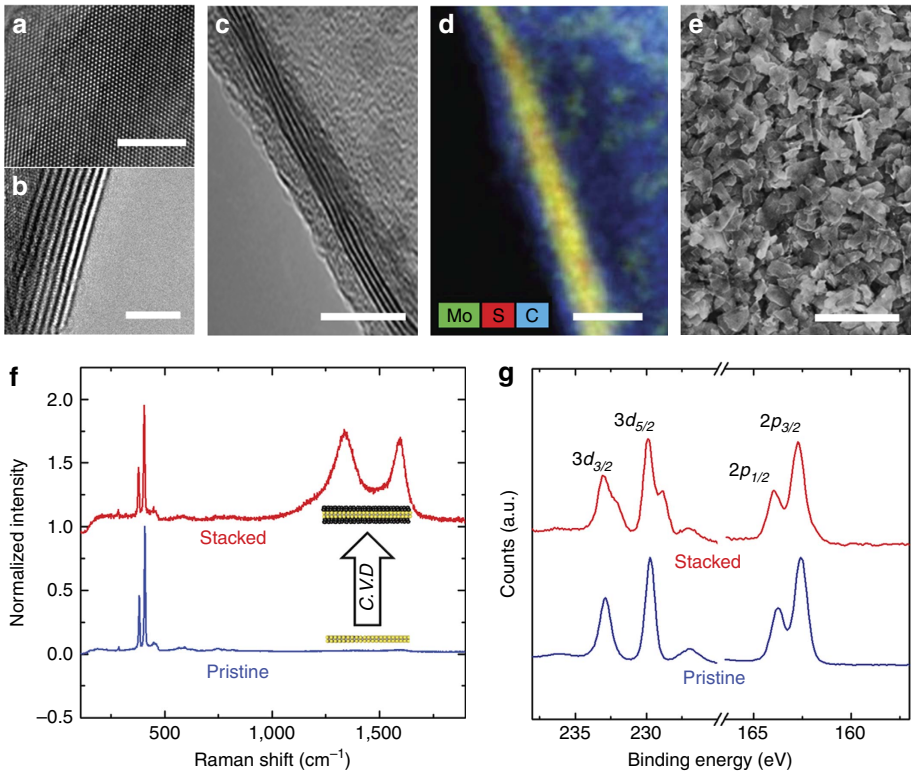

Figure 1 | Synthesis of vertically stacked carbon-MoS_2 heterostructured nanosheets. (**a**,**b**) TEM images of pristine exfoliated MoS_2 nanosheets. (**c**) Edge-view TEM image of a vertically stacked carbon-MoS_2 (C-MoS_2) nanosheet. (**d**) Energy-dispersive X-ray spectroscopy analysis of a stacked C-MoS_2 nanosheet. The coloured inset describes the colour assignment of each mapped element, overlapping Mo and S signals appear yellow in the image. (**e**) Scanning electron microscopy image of an electrophoretically assembled electrode material formed with stacked C-MoS_2 nanosheets. Scale bars, 4 nm (**a**,**b**) 10 nm (**c**,**d**) and 1 μm (**e**). (**f**) Raman spectroscopy and (**g**) X-ray photoelectron spectroscopy of pristine MoS_2 nanosheets and stacked C-MoS_2 nanosheets.

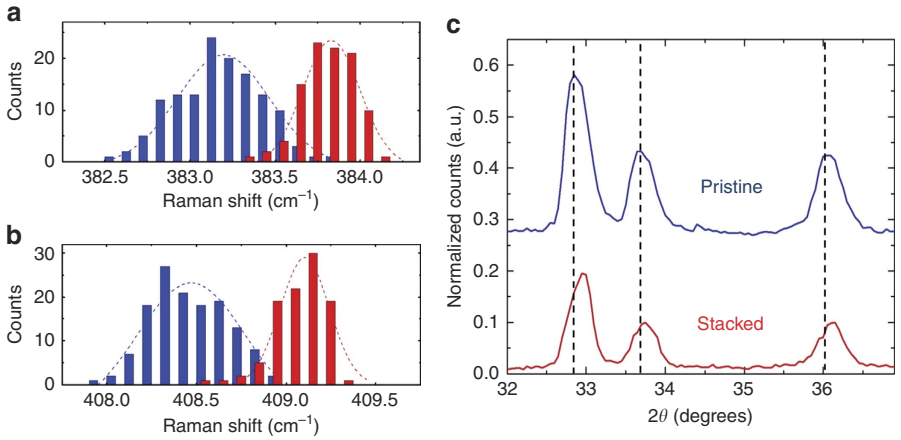

Figure 2 | Interface strain in vertically stacked 2D C-MoS_2 nanosheets. Distributions from Raman spectroscopy maps comprising >100 individual scans showing average shifts in the MoS_2 (**a**) E_{2g} and (**b**) A_{1g} modes due to strain induced by a lattice mismatched carbon-MoS_2 interface. The dotted lines overlaying each distribution represent Gaussian fits to the distribution data. (**c**) X-ray diffraction analysis of vertically stacked C-MoS_2 nanosheets indicating stacking-induced strain in low-index planes. The following planes can be assigned to the X-ray diffraction spectra: $2\theta = 32.6°$ is (100), $2\theta = 33.5°$ is (101) and $2\theta = 35.8°$ is (102). The vertical dotted lines emphasize the difference in peak positions between the two spectra.

properties against similar electrode materials produced with pristine MoS_2 nanosheets (Supplementary Figs 5,6, Supplementary Notes 4,5). Cyclic voltammetry scans of these electrodes and corresponding differential capacity plots based on galvanostatic measurements are shown in Fig. 3. As these two electrode materials differ only by the presence of a vertically stacked C-MoS_2 interface, electrochemical data indicates significant changes to the chemical processes occurring on lithium insertion into the MoS_2 material. For pristine MoS_2 nanosheets, two subsequent reactions are observed, with the first one at ~1.1 V and the second at ~0.55 V versus Li/Li^+. (Fig. 3a,b) This is consistent with the known pathways for insertion of lithium into pristine MoS_2, which occurs first through an intercalation reaction (1.1 V) that follows

$$MoS_2 + xLi^+ + xe^- \rightarrow Li_xMoS_2 \quad (1)$$

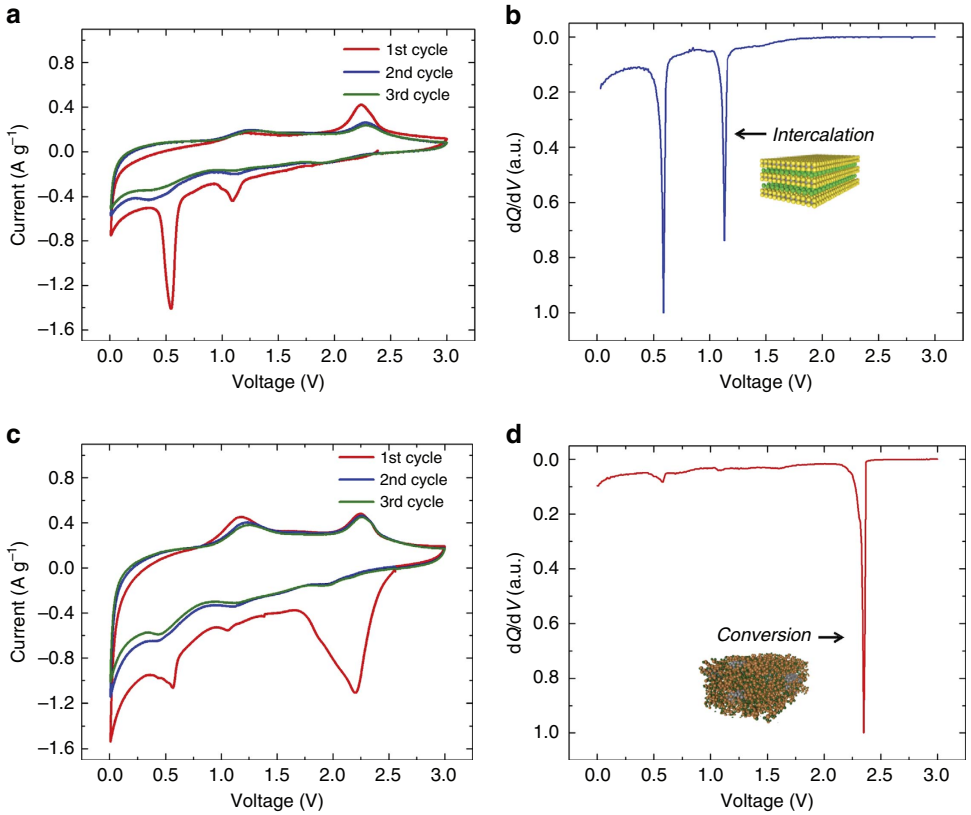

Figure 3 | Electrochemical assessment of strained carbon-MoS_2 heterostructured nanosheets. (**a**) CV and (**b**) normalized differential capacity measurements for MoS_2 under lithium insertion and extraction, with an arrow indicating the potential of the intercalation reaction that occurs in pristine MoS_2 materials. (**c**) CV and (**d**) normalized differential capacity plots for vertically stacked C-MoS_2 nanosheets, with an arrow indicating the electrochemical signature of direct chemical conversion.

where MoS_2 undergoes a transition from a semiconducting 2H phase to the metallic 1 T phase due to strain-induced deformation of the crystal from lithium ion insertion. Following this transition, the MoS_2 can undergo a subsequent conversion reaction at lower voltages (0.55 V) that follows

$$Li_xMoS_2 + 4Li^+ + 4e^- \rightarrow 2Li_2S + Mo/Li_y \qquad (2)$$

In contrast to this, insertion of lithium into the vertically stacked C-MoS_2 nanosheets yields a chemical reaction evident at $\sim$2.3 V versus Li/Li^+ based on both CV and diferential capacity curves (Fig. 3c,d) which is close to the open-circuit voltage (OCV) of the device. This reaction proceeds in the absence of Li intercalation into MoS_2 and no significant signature of lithium insertion at lower voltages occurs such as in pristine MoS_2 nanosheet electrodes. This highlights the presence of a chemical storage process occurring in vertically stacked C-MoS_2 materials that is not observed in pristine MoS_2 materials (Fig. 4a) and that interface-induced strain can directly trigger chemical conversion at practical voltages. It is important to note that these results distinguish the stacked C-MoS_2 configuration from simple mixtures of carbon nanomaterials and MoS_2 nanosheets which have been reported previously[38–42], in two key ways, namely that the grown carbon layer induces interface strain not possible in weakly adhered mechanically mixed materials that modulates the chemical reactivity of the MoS_2 nanosheet toward chemical conversion, and that the stacked configuration provides a physical barrier to inhibit polysulfide dissolution into the electrolyte in a manner consistent with a yolk-shell confinement strategy[43]. However, the benefits reported in other studies by combining MoS_2 and carbons through mixing are also maintained in our study as evidenced by galvanostatic studies indicating better rate capability and improved storage capacity at high rates for the C-MoS_2 electrodes (Supplementary Fig. 7). In addition, whereas the correlation between X-ray diffraction, Raman spectroscopy and XPS indicate the presence of strain due to the mismatch of in-plane lattice parameters of the stacked materials below the critical thickness, charge transfer effects between the C and MoS_2 materials can play a role in the origin of strain measured using these techniques. We also observe the lack of any electrochemical signature of lithium intercalation into the ultrathin carbon coating, implying that stacked C-MoS_2 nanosheets exhibit differences from pristine nanosheets that can be explained by compressive strain imposed on the 2D MoS_2 material.

To address the effect of the C-MoS_2 interface on the electrochemical properties during lithium insertion, Raman spectroscopy of the electrophoretically assembled MoS_2-based electrodes at different cathodic potentials was carried out (Fig. 4b). This analysis is possible due to the preparation of electrodes in a manner that does not require binder materials often used in conventional battery electrodes that can overwhelm the desired Raman spectroscopic features. At OCV conditions, both electrode materials exhibit only the native Raman modes of MoS_2. Cathodic scans from OCV conditions to 1.75 V versus Li/Li^+—an energy below the Li^+ insertion reaction observed for vertically stacked C-MoS_2 nanosheets, yields no change for the pristine MoS_2 nanosheets, but the emergence of a distinct Raman peak at 746 cm^{-1} is observed for the stacked C-MoS_2 nanosheets. This mode is due to the formation of lithium polysulfides (Li_2S_n for $4 \leq n \leq 8$) that can be attributed to chemical conversion of the MoS_2 into reaction products in a manner consistent with equation (2) (ref. 44). Correspondingly, a decrease of the MoS_2

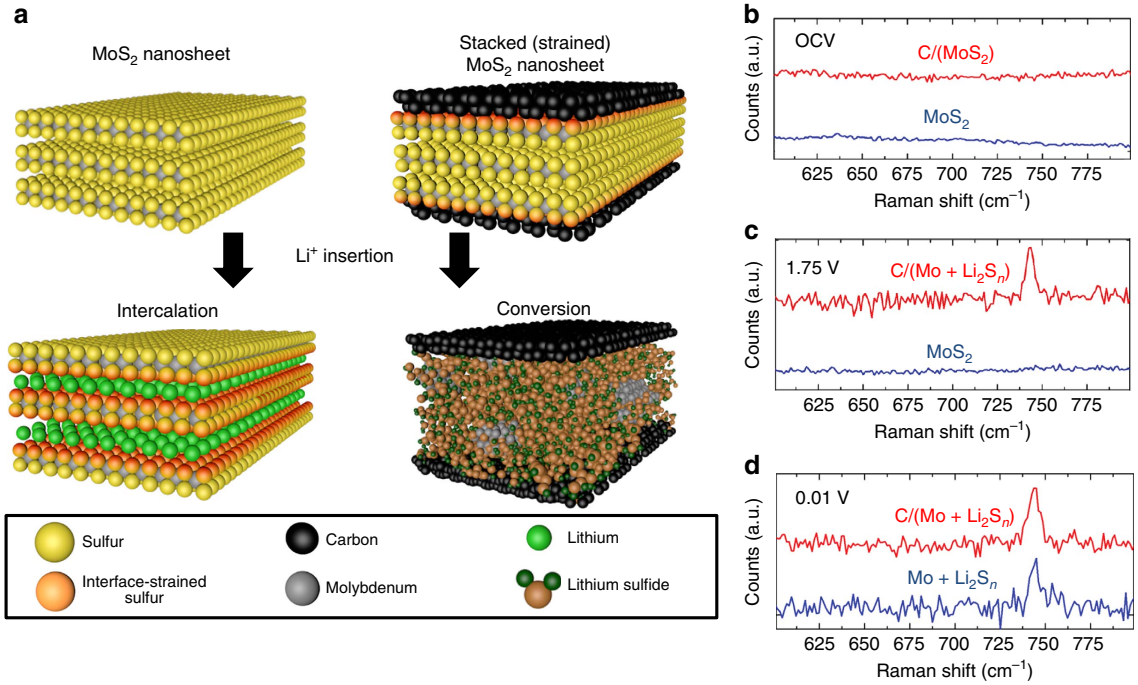

Figure 4 | Strain-induced modulation of chemical conversion in vertically stacked C-MoS_2 nanosheets. (**a**) Scheme showing the different chemical states between interface-strained MoS_2 nanosheets and pristine MoS_2 nanosheets after Li insertion, showing chemical conversion for stacked C-MoS_2 and intercalation for pristine MoS_2. *Ex situ* Raman spectroscopy confirming the electrochemical signature of chemical conversion based on the Raman mode of polysulfides at 746 cm^{-1} is presented for both materials at (**b**). Open-circuit voltage (OCV), (**c**) 1.75 V and (**d**) 0.01 V versus Li/Li^+. Notably, at 1.75 V versus Li/Li^+, the vertically stacked C-MoS_2 nanosheets have undergone chemical conversion, whereas the pristine MoS_2 nanosheets remain unconverted.

A_{1g} and E_{2g} modes are observed as expected from conversion (Supplementary Fig. 8, Supplementary Note 6). This confirms that the high voltage ~2.3 V signature in the CV and differential capacity curves for vertically stacked C-MoS_2 nanosheets (Fig. 3c,d) is a chemical conversion process similar to that which is known to occur at low voltages (0.55 V) in pristine MoS_2. To further support this, cathodic scans were continued down to 0.01 V versus Li/Li^+ for the pristine MoS_2 electrode, where the signature of conversion is evident due to the presence of the Raman mode at 746 cm^{-1}. Despite the difference in voltage of the conversion reactions between MoS_2 and C-MoS_2, similar Raman spectroscopic signatures of the polysulfide conversion product and similar post-conversion redox energetics in both cases implies that the resulting chemical state of the material in both conversion reactions is the same. To further support this, we performed *in situ* electrochemical impedance spectroscopy (EIS, Supplementary Fig. 9, Supplementary Table 1), where EIS analysis was performed at the same voltages as those assessed using Raman spectroscopy. EIS studies elucidate a picture consistent with Raman spectroscopy results that indicates the electrochemical signature of conversion in different voltage regimes for the pristine MoS_2 and the stacked C-MoS_2, respectively (Supplementary Note 7).

Discussion

On the basis of the combined spectroscopic and electrochemical analysis, a picture emerges emphasizing the role of interface strain on lithium insertion in vertically stacked C-MoS_2 materials. In the pristine semiconducting 2H phase of MoS_2, conversion of MoS_2 nanosheets cannot occur at voltages above where intercalation occurs (1.1 V versus Li/Li^+) and can only proceed in a two-step chemical process following an intercalation reaction. As many researchers have discussed the promise of MoS_2 nanosheets for battery cathodes, the requirement of a conversion reaction that is near the reduction potential of lithium is highly impractical in full-cell architectures. In a vertically stacked C-MoS_2 nanosheet, the interface strain due to lattice mismatch in a carbon-MoS_2 solid–solid interface leads to an average ~0.1% compressive strain that propagates into the MoS_2 nanosheet lattice and enables control of the energetics of chemical conversion. In this regard, interface strain provides the appropriate energetic landscape to sustain direct conversion at voltages that enable pairing with conventional anode materials such as silicon or graphite which give promise to practical incorporation of this device in a full-cell battery configuration. This distinctive difference in the chemical pathways achieved during lithium insertion as a result of interface strain is illustrated in Fig. 4a, where the chemical state of the 2D materials is drastically different following a cathodic scan to 1 V.

The broader use of controlled interface mechanics to modify chemical pathways in low-dimensional materials presents an unexplored horizon for engineered low-dimensional nanostructures. This utilizes 2D materials as a framework to merge concepts of strain engineering with mechanochemistry to control the energetics of chemical processes relevant to energy storage, energy conversion, catalysis, and sensing applications. Building from our results showing that strained interfaces in vertically stacked C-MoS_2 nanosheets can modulate electrochemical reactivity, we envision a new paradigm for material design that exploits interface strain and mechanics as a versatile toolbox to modulate performance of designer 2D materials in diverse applications.

Methods

MoS_2 nanosheet synthesis. In all, 500 mg of bulk MoS_2 powder (Aldrich, particle size < 2 μm) was added to 50 ml of 1-methyl-2-pyrrolidinone (Aldrich, 99.5% anhydrous). The solution was sonicated in a bath sonicator for 12 h using 8 × 90 min intervals. After sonication, the solution was centrifuged at 2,000 r.p.m. for 40 min. The upper 2/3 of the supernatant was removed and subsequently

centrifuged for 1 h at 5,000 r.p.m. before the excess supernatant was removed and the accumulated nanosheets were placed under vacuum overnight to completely evaporate the solvent.

Vertically stacked carbon-MoS_2 nanosheet synthesis. MoS_2 nanosheets contained within an alumina boat were placed into a 1-inch tube furnace and the tube was evacuated to 2 mTorr. A gas mixture of 100 standard cubic centimeters per minute (sccm) Ar and 20 sccm H_2 maintained at atmospheric pressure were introduced during ramping to a temperature 750 °C. At 750 °C, 2 sccm of acetylene (C_2H_2) was introduced for 10 min followed by a temperature ramp to 850 °C and an additional 10 min soak, and a final ramp to 950 °C for 10 min. After this process, the acetylene was turned off and the furnace cooled back down under a flow of argon and hydrogen, where materials were removed.

Electrophoretic deposition. A total of 20 mg of vertically stacked C-MoS_2 or pristine MoS_2 nanosheets were suspended in 20 ml NMP and sonicated for 30 min. Following this, a stainless steel spacer was placed at 0.5 cm from a 1×1 cm stainless steel counter electrode. A voltage of 30 V was applied for 30 min before carefully removing the coated steel electrode from solution and placing this into a vacuum chamber overnight to dry the sample.

Electrochemical device fabrication and testing. Electrochemical half-cell devices were assembled in an argon glovebox using CR 2,032 stainless steel coin cells purchased from MTI. The coated steel discs were separated from a lithium metal anode by a 2,500 Celgard separator saturated with a 1 M $LiPF_6$ in 1 g per 1 ml solution of ethylene carbonate and diethyl carbonate. Cyclic voltammetry scans and galvanostatic measurements were performed using a Metrohm autolab multichannel testing system.

Material characterization. Raman measurements were performed using a Renishaw inVia confocal Raman spectrometer. Micro-Raman maps were collected using a 532 nm laser. Before characterizing the electrodes after electrochemical testing, coin cells were disassembled in an Ar filled glovebox and the electrodes washed with an EC/DEC solution. TEM analysis was performed by drop casting a solution of pristine or stacked MoS_2 materials onto amorphous carbon TEM grids and then imaged using an FEI Osiris TEM at a beam voltage of 200 kV. X-ray diffraction was performed on powder samples using a Scintag XGEN 4,000 system with a CuKα (wavelength = 0.154 nm) radiation source. XPS was collected using a PHI 5,000 Versaprobe. Measurements were collected at a 45° takeoff angle with a 100 μm spot size with charge neutralization.

Data availability. The data that support the findings of this study are available from the corresponding author upon request.

References

1. Liu, J. H. & Liu, X. W. Two-dimensional nanoarchitectures for lithium storage. *Adv. Mater.* **24,** 4097–4111 (2012).
2. Gong, Y. J. *et al.* Vertical and in-plane heterostructures from WS_2/MoS_2 monolayers. *Nat. Mater.* **13,** 1135–1142 (2014).
3. Wang, X. & Xia, F. Van der Waals heterostructures: stacked 2D materials shed light. *Nat. Mater.* **14,** 264–265 (2015).
4. Yu, W. J. *et al.* Vertically stacked multi-heterostructures of layered materials for logic transistors and complementary inverters. *Nat. Mater.* **12,** 246–252 (2013).
5. Jariwala, D., Sangwan, V. K., Lauhon, L. J., Marks, T. J. & Hersam, M. C. Emerging device applications for semiconducting two-dimensional transition metal dichalcogenides. *ACS Nano* **8,** 1102–1120 (2014).
6. Britnell, L. *et al.* Strong light-matter interactions in heterostructures of atomically thin films. *Science* **340,** 1311–1314 (2013).
7. Hong, X. *et al.* Ultrafast charge transfer in atomically thin MoS_2/WS_2 heterostructures. *Nat. Nanotechnol.* **9,** 682–686 (2014).
8. Lee, G.-H. *et al.* Flexible and transparent MoS_2 field-effect transistors on hexagonal boron nitride-graphene heterostructures. *ACS Nano* **7,** 7931–7936 (2013).
9. Li, M.-Y. *et al.* Epitaxial growth of a monolayer WSe_2-MoS_2 lateral pn junction with an atomically sharp interface. *Science* **349,** 524–528 (2015).
10. Georgiou, T. *et al.* Vertical field-effect transistor based on graphene-WS_2 heterostructures for flexible and transparent electronics. *Nat. Nanotechnol.* **8,** 100–103 (2013).
11. He, J. *et al.* Electron transfer and coupling in graphene–tungsten disulfide van der Waals heterostructures. *Nat. Commun.* **5,** 5622 (2014).
12. Roy, K. *et al.* Graphene-MoS2 hybrid structures for multifunctional photoresponsive memory devices. *Nat. Nanotechnol.* **8,** 826–830 (2013).
13. Castellanos-Gomez, A. *et al.* Local strain engineering in atomically thin MoS_2. *Nano Lett.* **13,** 5361–5366 (2013).
14. He, K., Poole, C., Mak, K. F. & Shan, J. Experimental demonstration of continuous electronic structure tuning via strain in atomically thin MoS_2. *Nano Lett.* **13,** 2931–2936 (2013).
15. Liu, Z. *et al.* Strain and structure heterogeneity in MoS_2 atomic layers grown by chemical vapour deposition. *Nat. Commun.* **5,** 5246 (2014).
16. Desai, S. B. *et al.* Strain-induced indirect to direct bandgap transition in multi layer WSe_2. *Nano Lett.* **14,** 4592–4597 (2014).
17. Feng, J., Qian, X., Huang, C.-W. & Li, J. Strain-engineered artificial atom as a broad-spectrum solar energy funnel. *Nat. Photon.* **6,** 866–872 (2012).
18. Hwang, H., Kim, H. & Cho, J. MoS_2 nanoplates consisting of disordered graphene-like layers for high rate lithium battery anode materials. *Nano Lett.* **11,** 4826–4830 (2011).
19. Lacey, S. D. *et al.* Atomic force microscopy studies on molybdenum disulfide flakes as sodium-ion anodes. *Nano Lett.* **15,** 1018–1024 (2015).
20. Hu, L. R., Ren, Y. M., Yang, H. X. & Xu, Q. Fabrication of 3D hierarchical MoS_2/polyaniline and MoS_2/C architectures for lithium-ion battery applications. *ACS Appl. Mater. Inter.* **6,** 14644–14652 (2014).
21. Kibsgaard, J., Chen, Z., Reinecke, B. N. & Jaramillo, T. F. Engineering the surface structure of MoS_2 to preferentially expose active edge sites for electrocatalysis. *Nat. Mater.* **11,** 963–969 (2012).
22. Chou, S. S. *et al.* Understanding catalysis in a multiphasic two-dimensional transition metal dichalcogenide. *Nat. Commun.* **6,** 8311 (2015).
23. Wang, Y. *et al.* Monolayer $PtSe_2$, a new transition-metal-dichalcogenide, grown by direct selenization, shows promise for photocatalysis and valleytronics. *Nano Lett.* **15,** 4013–4018 (2015).
24. Sarkar, D. *et al.* MoS_2 field-effect transistor for next-generation label-free biosensors. *ACS Nano.* **8,** 3992–4003 (2014).
25. Perkins, F. K. *et al.* Chemical vapor sensing with monolayer MoS_2. *Nano Lett.* **13,** 668–673 (2013).
26. Lee, J. *et al.* Two-dimensional layered MoS_2 biosensors enable highly sensitive detection of biomolecules. *Sci. Rep.* **4,** 7352 (2014).
27. Shen, J. *et al.* Liquid phase exfoliation of two-dimensional materials by directly probing and matching surface tension components. *Nano Lett.* **15,** 5449–5454 (2015).
28. Nicolosi, V., Chhowalla, M., Kanatzidis, M. G., Strano, M. S. & Coleman, J. N. Liquid exfoliation of layered materials. *Science* **340,** 1226419 (2013).
29. Haar, S. *et al.* Enhancing the liquid-phase exfoliation of graphene in organic solvents upon addition of *n*-octylbenzene. *Sci. Rep.* **5,** 16684 (2015).
30. Du, M., Cui, L., Cao, Y. & Bard, A. J. Mechanoelectrochemical catalysis of the effect of elastic strain on a platinum nanofilm for the ORR exerted by a shape memory alloy substrate. *J. Amer. Chem. Soc.* **23,** 7397–7403 (2015).
31. Paton, K. R. *et al.* Scalable production of large quantities of defect-free few-layer graphene by shear exfoliation in liquids. *Nat. Mater.* **13,** 624–630 (2014).
32. Eda, G. *et al.* Photoluminescence from chemically exfoliated MoS_2. *Nano Lett.* **11,** 5111–5116 (2011).
33. Conley, H. J. *et al.* Bandgap engineering of strained monolayer and bilayer MoS_2. *Nano Lett.* **13,** 3626–3630 (2013).
34. Hui, Y. Y. *et al.* Exceptional tunability of band energy in a compressively strained trilayer MoS_2 sheet. *ACS Nano* **7,** 7126–7131 (2013).
35. Rice, C. *et al.* Raman-scattering measurements and first-principles calculations of strain-induced phonon shifts in monolayer MoS_2. *Phys. Rev. B.* **87,** 081307 (2013).
36. Lanzillo, N. A. *et al.* Temperature-dependent phonon shifts in monolayer MoS_2. *Appl. Phys. Lett.* **103,** 093102 (2013).
37. MacManus-Driscoll, J. L. Self-assembled heteroepitaxial oxide nanocomposite thin film structures: designing interface-induced functionality in electronic materials. *Adv. Funct. Mater.* **20,** 2035–2045 (2010).
38. Stephenson, T., Li, Z., Olsen, B. & Mitlin, D. Lithium ion battery applications of molybdenum disulfide (MoS_2) nanocomposites. *Energy Environ. Sci.* **7,** 209–231 (2014).
39. Chang, K. & Chen, W. L-cysteine-assisted synthesis of layered MoS_2/graphene composites with excellent electrochemical performances for lithium ion batteries. *ACS Nano* **5,** 4720–4728 (2011).
40. Jiang, H. *et al.* 2D monolayer MoS_2–carbon interoverlapped superstructure: engineering ideal atomic interface for lithium ion storage. *Adv. Mater.* **27,** 3687–3695 (2015).
41. Zhu, C., Mu, X., van Aken, P. A., Maier, J. & Yu, Y. Fast Li storage in MoS_2-graphene-carbon nanotube nanocomposites: advantageous functional integration of 0D, 1D, and 2D nanostructures. *Adv. Energy Mater.* **5,** 4 (2015).
42. Zhu, C., Mu, X., van Aken, P. A., Yu, Y. & Maier, J. Single-layered ultrasmall nanoplates of MoS_2 embedded in carbon nanofibers with excellent electrochemical performance for lithium and sodium storage. *Angew. Chem. Int. Ed.* **53,** 2152–2156 (2014).
43. Li, W. *et al.* High-performance hollow sulfur nanostructured battery cathode through a scalable, room temperature, one-step, bottom-up approach. *Proc. Natl Acad. Sci. USA* **110,** 7148–7153 (2013).

44. Yeon, J.-T. *et al.* Raman spectroscopic and X-ray diffraction studies of sulfur composite electrodes during discharge and charge. *J. Electrochem. Soc.* **159,** A1308–A1314 (2012).

Acknowledgements

We thank Nitin Muralidharan and Professor Rizia Bardhan for insightful discussions. This work was supported by the National Science Foundation under CMMI grant #1334269 and Vanderbilt start-up funds. TEM images were obtained from an instrument made possible by NSF grant EPS 1004083. A.P.C. and K.S. are supported by an NSF graduate fellowship under grant # 1445197.

Author contributions

L.O. and C.L.P jointly conceived the project and designed the experiments. L.O. and T.H. performed material fabrication with insights from K.S., and L.O. carried out device testing and performance analysis. R.C. performed TEM imaging and analysis, and A.P.C. performed X-ray diffraction measurements and analysis. B.S. performed XPS measurements and analysis. L.O. and C.L.P. wrote the manuscript and all authors participated in discussion and reviewed the manuscript before submission.

Additional information

Supplementary Information accompanies this paper at http://www.nature.com/naturecommunications

Competing financial interests: The authors declare no competing financial interests.

Reprints and permission information is available online at http://npg.nature.com/reprintsandpermissions/

How to cite this article: Oakes, L. *et al.* Interface strain in vertically stacked two-dimensional heterostructured carbon-MoS_2 nanosheets controls electrochemical reactivity. *Nat. Commun.* 7:11796 doi: 10.1038/ncomms11796 (2016).